Journal of Solid Mechanics Vol. 11, No. 3 (2019) pp. 615-634
DOI: 10.22034/JSM.2019.666691

Natural Frequency and Dynamic Analyses of Functionally Graded Saturated Porous Beam Resting on Viscoelastic Foundation Based on Higher Order Beam Theory

M. Babaei [1], K. Asemi [2,*], P. Safarpour [1]

[1] *Department of Mechanical Engineering, Shahid Beheshti University, Tehran, Iran*
[2] *Department of Mechanical Engineering, Islamic Azad University, Tehran North Branch, Tehran, Iran*

Received 21 June 2019; accepted 21 August 2019

ABSTRACT

In this paper, natural frequencies and dynamic response of thick beams made of saturated porous materials resting on viscoelastic foundation are investigated for the first time. The beam is modeled using higher-order beam theory. Kelvin-Voight model is used to model the viscoelastic foundation. Distribution of porosity along the thickness is considered in two different patterns, which are symmetric nonlinear and nonlinear asymmetric distributions. The relationship between stress and strain is based on the Biot constitutive law. Lagrange equations are used to express the motion equations. Finite element and Newark methods are used to solve the governing equations. The effect of different boundary conditions and various parameters such as porosity and Skempton coefficients, slenderness ratio as well as stiffness and damping coefficients of viscoelastic foundation on natural frequency and transient response of beam have been studied. Results show that in a drained condition, beam has smallest fundamental frequency and by increasing the Skempton coefficient, the fundamental frequency of the beam increases.

Keywords: Saturated porous beam; Functionally graded; Third order beam theory; Dynamic analysis; Viscoelastic foundation; Biot model.

1 INTRODUCTION

NOWADAYS porous media is applied in an astonishingly large body of applications, including petroleum geophysics, geotechnical engineering, civil engineering, hydrology, geology engineering and biomechanics. In most of these applications, theory of poroelasticity is commonly exploited to examine the raised problems. Porous material consists of a porous matrix and of a fluid in the pores of the matrix that is called pore fluid [1]. Biot [2] is the pioneer who has studied the poroelasticity. In his model, a porous material is composed of two phases namely

*Corresponding author.
E-mail address: K.asemi@iau-tnb.ac.ir (K. Asemi).

solid and fluid. The linear poroelasticity theory of Biot has two characteristics: 1- An increase of pore pressure induces a dilation of pore. 2- Compression of the pore causes a rise of pore pressure. There are several theories have also been developed for pore materials, but in practice they do not offer any advantage over the Biot theory.

During the last several years, porous material structures such as beams, plates, and shells have been used widely in structural design problems. Most of current studies are focused on the problem of deflection, buckling and vibrations of porous beams and plates which some of them are referred in here. Theodorakopoulos and Beskos [3] have extended the classical theory of thin rectangular plates to porous materials including Biot's stress-strain relations in porous media. They have established two coupled governing equations and have given the solutions for a simply supported plate by extending Navier's algebraic solution to the porous case. Leclaire et al. [4] presented the vibrations of a rectangular porous plate described by two coupled equations involving the time and space derivatives of the deflection and of the relative fluid-solid motion. By using Galerkin's variational method and classical theory of plates, the equations were solved. Buckling of porous beams with varying properties was described by Magnucki and Stasiewicz [5]. They used shear deformation theory for solving the critical load, and also they have investigated the effect of porosity on the strength and buckling load of the beam. Magnucka-Blandzi [6] investigated the problem of axi-symmetrical deflection and buckling of circular porous–cellular plate with the geometric model of nonlinear hypothesis. Magnucka-Blandzi and Magnucki [7] performed an effective design of a sandwich beam with an FG metal foam core and calculated the optimal dimensionless parameters to maximize the critical force and minimize the beam mass. Debowski and Magnucki [8] explored the dynamic stability of a porous rectangular plate to study an axial compressed porous-cellular rectangular plate which is a generalization of sandwich or multilayer plates. Mojahedin et al. [9] carried out the study of thermal and mechanical stability of solid circular plates made of saturated/unsaturated FG porous materials with piezoelectric actuators by employing the energy method and classical plate theory. Jabbari et al. [10] investigated the buckling analysis of radially loaded functionally graded solid circular saturated porous plate. They derived the equilibrium and stability equations through the variational formulation based on Sander's nonlinear strain-displacement relation. They came to the conclusion that increasing porosity decreases buckling load. They also found that the Monotonous porosity is more unstable than symmetric and non-symmetric porosity and the critical buckling load will be reduced by increasing the compressibility of fluid within the pores. Jabbari et al. [11] investigated buckling analysis of thin circular FG plates made of saturated porous-soft ferromagnetic materials in transverse magnetic field. Ebrahimi and Mokhtari [12] studied vibrational behavior of a rotating porous FG beam by using DQM and Euler Bernoulli beam theory. Ebrahimi and Jafari [13] and Ebrahimi et al. [14] analyzed thermo-mechanical vibrations of FG porous beams under various thermal loadings by employing a semi-analytical differential transform method based on four variable refined shear deformation beam theory and Euler Bernoulli beam theory, respectively. Chen et al. [15, 16] by using Timoshenko beam theory presented the elastic buckling, static bending, free and forced vibration analyses of shear deformable FG porous beams made of open-cell metal foams with two poro/nonlinear non-symmetric distribution, poro/nonlinear symmetric distribution and compared the influences from different porosity distributions. Chen et al. [17] studied nonlinear free vibration of shear deformable sandwich beam based on Timoshenko beam theory. In [12- 17], the constitutive equations are based on Hooke's law or the behavior of porous structure in drained condition is studied. Arshid and Khorshidvand [18] studied free vibration analysis of saturated porous FG circular plates integrated with piezoelectric actuators via differential quadrature method. Using Hamilton's variational principle and the classical plate theory, the governing motion equations have been obtained. Galeban et al. [19] studied free vibration of functionally graded thin beams made of saturated porous materials. The equations of motion were derived using Euler-Bernoulli theory and natural frequencies of porous beam have been obtained for different boundary conditions. The effects of poroelastic parameters and pores compressibility has been considered on the natural frequencies. Grygorowicz et al. [20] employed a broken line hypothesis and a nonlinear hypothesis to conduct analytical and numerical studies on the elastic buckling of a sandwich beam with FG metal core. Based on the Reddy's third-order shear deformation theory, the dynamic characteristics of a porous rectangular plate resting on a Pasternak foundation was solved by differential quadrature method [21]. Arani et al [22] used third order shear deformation theory and differential quadrature method (DQM) to investigate the natural vibration of porous plate. They also investigated nonlocal free vibration analysis of FG-porous shear and normal deformable sandwich nanoplate with piezoelectric face sheets resting on silica aerogel foundation [23].

Porous beam has wide application and can be used in aerospace industry as a vibration damper, in sea structures and in submarines due to its very low density and in reformer and catalysts due to the high specific surface. Therefore, it is important to study the behavior of these structures. The above literature review shows that the analysis of porous beams has mainly been performed based on the simple beam theories (Euler and Timoshenko), and Hooke's law or drained condition is considered to model the porous behavior of beam. In this paper, free and transient vibration of a thick saturated porous functionally graded beam resting on a viscoelastic foundation has been

investigated based on the third order shear deformation theory and Biot constitutive law which has not been surveyed so far. Kelvin- voight model is used to model the viscoelastic foundation. Distribution of porosity along the thickness is considered in two different patterns, which are symmetric nonlinear and nonlinear asymmetric distributions. Lagrange equations are used to express the motion equations and the finite element and Newark methods are used to solve the governing equation. The effect of different boundary conditions and various parameters such as Biot, porosity and Skempton coefficients and slenderness ratio as well as stiffness and damping coefficients of viscoelastic foundation on natural frequency and transient response of beam in undrained condition have been studied.

2 DERIVATION OF THE GOVERNING EQUATIONS

Consider a beam made of saturated porous materials with rectangular cross section resting on a viscoelastic foundation. It is assumed that the length of the beam is L and cross section is $b \times h$. Cartesian coordinates is used such that the x axis is at the left side of the beam on its middle surface (Fig.1).

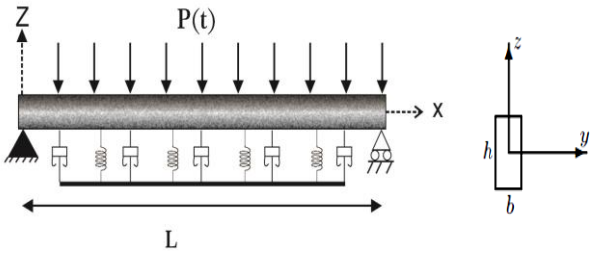

Fig.1
Beam on viscoelastic foundation.

Mechanical properties of the porous material vary across the thickness of the beam. Two different distributions of a porous beam are as follow and are shown in Fig.2:

a) Porous material with nonlinear non-symmetric distribution (PNND): material which has nonlinear asymmetric distribution of porosity in thickness direction. Shear modulus, Young's modulus and density for PNND are as [24, 25]:

$$\begin{aligned} G(z) &= G_1\left[1-e_0 cos\left(\left(\frac{\pi}{2*h}\right)\left(z+\frac{h}{2}\right)\right)\right] \\ E(z) &= E_1\left[1-e_0 cos\left(\left(\frac{\pi}{2*h}\right)\left(z+\frac{h}{2}\right)\right)\right] \\ \rho(z) &= \rho_1\left[1-e_m cos\left(\left(\frac{\pi}{2*h}\right)\left(z+\frac{h}{2}\right)\right)\right] \end{aligned} \quad (1)$$

b) Porous material with nonlinear symmetric distribution (PNSD): material which has nonlinear symmetric distribution of porosity in thickness direction. Young's modulus, shear modulus and density for PNSD are as [26]:

$$\begin{aligned} E(z) &= E_1\left[1-e_0 cos\left(\left(\frac{\pi z}{h}\right)\right)\right] \\ G(z) &= G_1\left[1-e_0 cos\left(\left(\frac{\pi z}{h}\right)\right)\right] \\ \rho(z) &= \rho_1\left[1-e_m cos\left(\left(\frac{\pi z}{h}\right)\right)\right] \end{aligned} \quad (2)$$

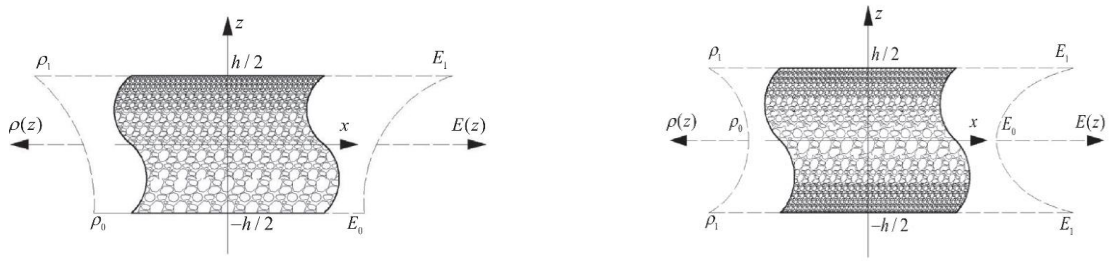

(a) PNND (b) PNSD

Fig.2
Two different distributions of a porous beam.

where for two different porosity distributions, we have:

$$e_0 = 1 - \frac{G_0}{G_1} = 1 - \frac{E_0}{E_1}$$
$$e_m = 1 - \sqrt{1 - e_0} \tag{3}$$

where e_0 is the coefficient of plate porosity ($0<e_0<1$). For PNND, E_0 and E_1 are Young's modulus of elasticity at $z=-h/2$ and $z=h/2$, respectively. Also, G_0 and G_1 are the shear modulus at $z=-h/2$ and $z=h/2$, respectively. The relationship between the modulus of elasticity and shear modulus is $E_j = 2G_j(1+\nu)$ ($j=0,1$) and ν is Poisson's ratio, which is assumed to be constant across the beam thickness.

2.1 Constitutive equations

Constitutive equations of porous beam are based on Biot theory instead of Hook's law. The linear poroelasticity theory of Biot has two characteristics [2]

1) An increase of pore pressure induces a dilation of pore.
2) Compression of the pore causes a rise of pore pressure.

The stress-strain law for the Biot poroelasticity is given by [27].

$$\sigma_{ij} = 2G\varepsilon_{ij} + \lambda\varepsilon_{kk}\delta_{ij} - p\alpha\delta_{ij}$$
$$p = \bar{M}\left(\varsigma - \alpha\varepsilon_{kk}\right)$$
$$\bar{M} = \frac{2G\left(\nu_u - \nu\right)}{\alpha^2\left(1-2\nu_u\right)\left(1-2\nu\right)} \tag{4}$$
$$\nu_u = \frac{\nu + \alpha\beta\left(1-2\nu\right)/3}{1 - \alpha\beta\left(1-2\nu\right)/3}$$

Here p is pore fluid pressure, $\bar{M}$ is Biot's modulus, G is shear modulus, ν_u is undrained Poisson's ratio ($\nu<\nu_u<0/5$), α is the Biot coefficient of effective stress ($0<\alpha<1$), ε_{kk} is the volumetric strain, ς is variation of fluid volume content, β is Skempton coefficient. For $p=0$, the Biot law reduces to conventional Hook's law or drained condition.

The pore fluid property is introduced by the Skempton coefficient. The Biot's coefficient (α) describes the porosity effect on the behavior of the porous material without fluid, and states that due to porosity, the resistance of the body varies a few percent and is defined as follows:

$$\alpha = 1 - \frac{K}{K_S} \tag{5}$$

where K_S is the bulk modulus of a homogeneous material. The relationship between the bulk mdulus and the shear modulus is as follows:

$$K = \frac{2(1+v)}{3(1-2v)}G$$
$$K_u = \frac{2(1+v_u)}{3(1-2v_u)}G \tag{6}$$

The Skempton coefficient is a measure of the relative compressibility between solid and fluid. The Skempton coefficient is an important dimensionless parameter for describing the effect of the fluid inside the cavities on the behavior of the porous material in the undrained state ($\varsigma = 0$), and is the ratio of the cavity pressure to the total body stress.

$$\beta = \frac{dp}{d\sigma}|_{\zeta=0} = \frac{1}{1+e_0 \frac{C_P}{C_s}} = \frac{K_u - K}{\alpha K_u} \tag{7}$$

where K_u is the bulk modulus in the undrained state, K is the bulk modulus in the drained state, C_P is the fluid Compressibility in the pores and C_s is solid Compressibility. The Skempton coefficient also shows the effect of fluid Compressibility on the elastic modulus and the compressibility of the entire porous material [28].

2.2 Displacement field and strain

The displacement field based on the third order beam theory of Reddy [29] is given by:

$$u(x,z,t) = u_0(x,t) + z\,\Phi_x(x,t) - 4\frac{z^3}{3h^2}\left[\Phi_x(x,t) + \frac{\partial w_0(x,t)}{\partial x}\right] \tag{8}$$

$$w(x,z,t) = w_0(x,t) \tag{9}$$

where u and w are the displacement components in the x and z directions respectively. u_0 and w_0 are the midplane displacements and Φ_x is the bending rotation of x-axis. t denotes time and h is the total thickness of the beam. The matrix form of the displacement field is as:

$$\bar{u} = \begin{bmatrix} u \\ w \end{bmatrix} = \begin{bmatrix} 1 & 0 & -4\frac{z^3}{3h^2} & \left(z - 4\frac{z^3}{3h^2}\right) \\ 0 & 1 & 0 & 0 \end{bmatrix} \begin{bmatrix} u_0 \\ w_0 \\ \frac{\partial w_0}{\partial x} \\ \Phi_x \end{bmatrix} = [Z_c][\bar{U}] \tag{10}$$

where

$$[\bar{U}] = \begin{bmatrix} u_0 \\ w_0 \\ \frac{\partial w_0}{\partial x} \\ \Phi_x \end{bmatrix} \qquad [z_c] = \begin{bmatrix} 1 & 0 & -4\frac{z^3}{3h^2} & \left(z - 4\frac{z^3}{3h^2}\right) \\ 0 & 1 & 0 & 0 \end{bmatrix} \tag{11}$$

The strain–displacement relations can be described in a matrix form as:

$$[\varepsilon]=\begin{bmatrix}\varepsilon_{xx}\\ \gamma_{xz}\end{bmatrix}=\begin{bmatrix}1 & \left(z-4\frac{z^3}{3h^2}\right) & -4\frac{z^3}{3h^2} & 0\\ 0 & 0 & 0 & \left(1-4\frac{z^2}{h^2}\right)\end{bmatrix}\begin{bmatrix}\frac{\partial u_0}{\partial x}\\ \frac{\partial \Phi_x}{\partial x}\\ \frac{\partial^2 w_0}{\partial x^2}\\ \Phi_x+\frac{\partial w_0}{\partial x}\end{bmatrix}=[Z]\left[\bar{\varepsilon}\right] \tag{12}$$

where $\left[\bar{\varepsilon}\right]$ is expressed in the following equation:

$$[\bar{\varepsilon}]=\begin{bmatrix}\frac{\partial}{\partial x} & 0 & 0 & 0\\ 0 & 0 & 0 & \frac{\partial}{\partial x}\\ 0 & \frac{\partial^2}{\partial x^2} & 0 & 0\\ 0 & 0 & 1 & 1\end{bmatrix}\left[\bar{U}\right]=[d]\left[\bar{U}\right] \tag{13}$$

So, $[\varepsilon]$ can be presented in the following matrix form:

$$[\varepsilon]=[Z][d]\left[\bar{U}\right] \tag{14}$$

The stress- strain relationship for a porous beam in an undrained condition ($\varsigma=0$) is as follows:

$$[\sigma]=[D][\varepsilon] \tag{15}$$

where $[\sigma]$, $[\varepsilon]$, $[D]$ and its components are:

$$[\sigma]=[\sigma_{xx}\quad \sigma_{xz}]^T \tag{16}$$

$$[D]=\begin{bmatrix}Q_{11}(z) & 0\\ 0 & Q_{55}(z)\end{bmatrix} \tag{17}$$

$$Q_{11}(z)=\frac{E(z)}{1-\nu^2}+\bar{M}\alpha^2 \tag{18}$$

$$Q_{55}(z)=G(z) \tag{19}$$

In this research, the beam is supported by viscoelastic foundation. The Kelvin-voight linear model is used for modeling of the viscoelastic foundation. The relationship between force per unit area and deflection in this model can be calculated according to the following equation [30]:

$$P\left(x,t\right)=k_w w\left(x,t\right)+c_d\frac{\partial w\left(x,t\right)}{\partial t} \tag{20}$$

where k_w is the elastic coefficient of the foundation in terms of (N/m^3), and c_d is the damping coefficient of the foundation in terms of ($N.s/m^3$).

2.3 Finite element model of governing equations

The approximation of the displacement field in each element of the beam is as follows:

$$\left[\bar{U}^{(e)}\left(x,t\right)\right]=\left[N\left(x\right)\right]\left[Q^{(e)}\left(t\right)\right] \tag{21}$$

$\left[Q^{(e)}\left(t\right)\right]$ is nodal degrees of freedom of the beam element and $\left[N\left(x\right)\right]$ is shape function matrix and its components are shown in the appendix. $\left[Q^{(e)}\left(t\right)\right]$ contains $u_i, w_i, \frac{\partial w_i}{\partial x}$ and Φ_i. For u_i and Φ_i, the linear approximation is used and for approximation of w_i and $\frac{\partial w_i}{\partial x}$, the Hermitian element of the Euler-Bernoulli beam is used. By replacing the Eq. (21) in (13):

$$\left[\bar{\varepsilon}\right]=\left[B\right]\left[Q^{(e)}\right] \tag{22}$$

In which [B]=[d] $\left[\mathrm{N(x)}\right]$ represents the derivative of the matrix of the shape functions in terms of x and is explained in the appendix. The velocity components are obtained from the time derivative of the displacement field as follows:

$$\left[\dot{\bar{U}}\right]=\left[N\left(x\right)\right]\left[\dot{Q}^{(e)}\left(t\right)\right] \tag{23}$$

where $\left[\dot{Q}^{(e)}\left(t\right)\right]$ is the velocity component of element nodes.

The equation of motion of is extracted by using the Lagrange equations as follows:

$$\left\{\frac{d}{dt}\left(\frac{\partial T}{\partial \dot{Q}}\right)\right\}+\left\{\frac{\partial R}{\partial \dot{Q}}\right\}+\left\{\frac{\partial U}{\partial Q}\right\}=F \tag{24}$$

In the above equation, kinetic energy is a function of the dissipation of the Rayleigh and the total potential energy and the total force on the beam. The kinetic energy and the total potential energy are defined as follow:

$$\begin{aligned} T^{(e)} &= \frac{1}{2}\iiint [\dot{\bar{U}}]^T\,[Z_C]^T\,\rho(Z)][Z_C][\dot{\bar{U}}]dxdydz \\ &= \frac{1}{2}b\int_0^{l^{(e)}} [\dot{\bar{U}}]^T\left(\int_{-h/2}^{h/2}[Z_C]^T\,\rho(Z)[Z_C]dz\right)[\dot{\bar{U}}]dx \\ &= \frac{1}{2}b\int_0^{l^{(e)}} [\dot{Q}^{(e)}]^T\,[N]^T[\bar{Z}][N][\dot{Q}^{(e)}]dx \end{aligned} \tag{25}$$

Total potential energy of system is as:

$$U^{(e)} = U_1^{(e)} + U_2^{(e)} = \frac{1}{2}\int \varepsilon^T \sigma dV + \frac{1}{2}\iint k_w w^2 dxdy$$
$$= \frac{1}{2} b \int_0^{l^{(e)}} \int_{-h/2}^{h/2} \left[Q^{(e)}\right]^T [B]^T [Z]^T [D][Z][B] \left[Q^{(e)}\right] dx\, dz + \frac{1}{2} b \int_0^{l^{(e)}} \left[Q^{(e)}\right]^T \left[\bar{N}\right]^T k_w \left[\bar{N}\right] \left[Q^{(e)}\right] dx \quad (26)$$
$$= \frac{1}{2}\left[Q^{(e)}\right]^T \left(b \int_0^{l^{(e)}} [B]^T \left[\bar{D}\right][B] dx \right) \left[Q^{(e)}\right] + \frac{1}{2}\left[Q^{(e)}\right]^T \left(b \int_0^{l^{(e)}} \left[\bar{N}\right]^T k_w \left[\bar{N}\right] dx \right) \left[Q^{(e)}\right]$$

$[\bar{Z}]$ and $[\bar{D}]$ are defined as follow and $\bar{N}$ is presented in appendix:

$$\left[\bar{D}\right] = \int_{-\frac{h}{2}}^{\frac{h}{2}} [Z]^T [D][Z] dz$$
$$\left[\bar{Z}\right] = \int_{-h/2}^{h/2} \left[Z_c\right]^T \rho(z) \left[Z_c\right] dz \quad (27)$$

Since the damping of the viscoelastic foundation is a function of the Rayleigh dissipation (R). So, the equation of Rayleigh dissipation matrix for each element of the beam is:

$$R^{(e)} = \frac{1}{2} \iint c_d \dot{w}^2 dx\, dy =$$
$$\frac{1}{2} b \int_0^{l^{(e)}} \left[\dot{Q}^{(e)}\right]^T \left[\bar{N}\right]^T c_d \left[\bar{N}\right] \left[\dot{Q}^{(e)}\right] dx = \frac{1}{2}\left[\dot{Q}^{(e)}\right]^T \left(b \int_0^{l^{(e)}} \left[\bar{N}\right]^T c_d \left[\bar{N}\right] dx \right) \left[\dot{Q}^{(e)}\right] \quad (28)$$

If $p_z(t)$ is the external force of the beam, the work performed is defined by Eq. (29):

$$W_f^{(e)} = \frac{1}{2}\iint \begin{bmatrix} 0 \\ p_z \\ 0 \\ 0 \end{bmatrix} w\, dA = \frac{1}{2}\left[Q^{(e)}\right]^T \left(b \int_0^{l^{(e)}} \left[\bar{N}\right]^T \begin{bmatrix} 0 \\ p_z \\ 0 \\ 0 \end{bmatrix} dx \right) \quad (29)$$

Therefore, the mass matrix $\left[M^{(e)}\right]$, The stiffness matrix caused by strain $\left[K_\varepsilon^{(e)}\right]$, the stiffness matrix due to the elastic properties of the foundation $\left[K_{kw}^{(e)}\right]$, the damping matrix due to damping property of foundation $\left[C^{(e)}\right]$ and the external force matrix for each element of the beam $\left\{F^{(e)}\right\}$ are as following:

$$\left[M^{(e)}\right] = b \int_0^{l^{(e)}} [N]^T \left[\bar{Z}\right][N] dx \quad (30)$$

$$\left[K_\varepsilon^{(e)}\right] = b \int_0^{l^{(e)}} [B]^T \left[\bar{D}\right][B] dx \quad (31)$$

$$\left[K_{kw}^{(e)}\right] = b \int_0^{l^{(e)}} \left[\bar{N}\right]^T k_w \left[\bar{N}\right] dx \quad (32)$$

$$\left[C^{(e)}\right]=b\int_0^{l^{(e)}}\left[\bar{N}\right]^T c_d\left[\bar{N}\right]dx \tag{33}$$

$$\left\{F^{(e)}\right\}=b\int_0^{l^{(e)}}\left[\bar{N}\right]^T\begin{bmatrix}0\\ p_z\\ 0\\ 0\end{bmatrix}dx \tag{34}$$

After assembly of element matrices, the matrix form of the Lagrange equations is as:

$$[M]\left[\ddot{Q}\right]+[C]\left[\dot{Q}\right]+[K][Q]=\{F\} \tag{35}$$

To solve the governing equations in time domain, Newmark integration method is used [31]. In this method, the displacement and velocity vectors at time $t+\Delta t$ are approximated in terms of their values at time *t* according to the following equations:

$$\left\{\dot{Q}\right\}_{t+\Delta t}=\left\{\dot{Q}\right\}_t+\left[(1-\gamma)\left\{\ddot{Q}\right\}_t+\gamma\left\{\ddot{Q}\right\}_{t+\Delta t}\right]\Delta t \tag{36}$$

$$\{Q\}_{t+\Delta t}=\{Q\}_t+\left\{\dot{Q}\right\}_t\Delta t\left[\left(\frac{1}{2}-\beta\right)\left\{\ddot{Q}\right\}_t+\beta\left\{\ddot{Q}\right\}_{t+\Delta t}\right]\Delta t^2 \tag{37}$$

By choosing the parameters $\beta=1/4$ and $\gamma=1/2$, the solution method is called the mean acceleration method and is unconditionally stable in linear analysis. Now the equilibrium Eq. (35) for time is rewritten as follows:

$$[M]\left\{\ddot{Q}\right\}_{t+\Delta t}+[C]\left\{\dot{Q}\right\}_{t+\Delta t}+[K]\{Q\}_{t+\Delta t}=\{F\}_{t+\Delta t} \tag{38}$$

From the solution of Eq. (37), $\left\{\ddot{Q}\right\}_{t+\Delta t}$ is obtained and $\left\{\dot{Q}\right\}_{t+\Delta t}$ is obtained by replacing $\left\{\ddot{Q}\right\}_{t+\Delta t}$ in Eq. (36). Now $\left\{\ddot{Q}\right\}_{t+\Delta t}$ and $\left\{\dot{Q}\right\}_{t+\Delta t}$ are obtained in terms of $\{Q\}_{t+\Delta t}$, and by replacing these expressions in Eq. (38), the following relation is obtained:

$$\left[\tilde{K}\right]\{Q\}_{t+\Delta t}=\left\{\tilde{F}\right\} \tag{39}$$

In the above equation, the matrices $\left[\tilde{K}\right]$ and $\left\{\tilde{F}\right\}$ are defined as follows:

$$\begin{aligned}\left[\tilde{K}\right]&=\frac{1}{\beta\Delta t^2}[M]+[K]+\frac{\lambda}{\beta\Delta t}[C]\\ \left[\tilde{F}\right]&=\{F\}_{t+\Delta t}+[M]\left(\frac{1}{\beta\Delta t^2}\{Q\}_t+\frac{1}{\beta\Delta t}\left\{\dot{Q}\right\}_t+\left(\frac{1}{2\beta}-1\right)\left\{\ddot{Q}\right\}_t\right)\\ &+[C]\left(\frac{\gamma}{\beta\Delta t}\{Q\}_t+\left(\frac{\gamma}{\beta}-1\right)\left\{\dot{Q}\right\}_t+\frac{\Delta t}{2}\left(\frac{\gamma}{\beta}-1\right)2\left\{\ddot{Q}\right\}_t\right)\end{aligned} \tag{40}$$

with the known initial conditions and marching through time, the Eq. (40) is solved and displacements at each time are obtained.

3 NUMERICAL RESULTS

In this section, numerical results have been obtained for free and transient vibration of porous beam in undrained condition. The effects of different boundary conditions, porosity distribution, porosity parameters and slenderness ratio have been investigated. The material properties of the porous beam are considered as: $E_1 = 200GPa$, $\rho_1 = 7850kg/m^3$ and $v = 1/3$.

Natural frequencies have been normalized by the following relation:

$$\omega = \Omega L \sqrt{\frac{\rho_1}{E_1} * \left(1 - v^2\right)} \tag{41}$$

where Ω is the natural frequency and ω is dimensionless form of natural frequency.

3.1 Free vibration

To validate the results of present study, natural frequencies of a porous beam with different boundary conditions and for two porosity distributions and different slender ratio (*L/h*) are obtained and compared with results of [16] in Tables 1 and 2. Comparison of results shows excellent agreement between them. In [16], Hook's law (drained condition) and Timoshenko beam theory is used to model the dynamic behavior of porous beam, while in the present study, Reddy beam theory and Biot constitutive law are used. To derive results of Ref. [16] in the present study, Skempton coefficient is considered to be zero. This assumption gives $V_u = V$, Biot's modulus $\bar{M} = 0$ and pore fluid pressure $p = 0$. Table 2., denotes that by increasing the porosity coefficient, fundamental natural frequency for PNSD is increased and for PNND is decreased. This is due to the fact that by increasing the porosity coefficient, free space of the beam increases and both of stiffness and mass matrices decrease, but the rate of reduction in stiffness matrix is smaller than that of mass matrix for PNSD, while this is just the opposite for PNND.

Table 1
Fundamental natural frequency for different boundary conditions, *L/h* and porosity distribution compared with [16] for *e*0=0.5.

	PNSD		PNND	
L/h	[16]	present	[16]	present
	H–H beam		H–H beam	
10	0.2798	0.2792	0.2599	0.2598
20	0.1422	0.1421	0.1318	0.1318
50	0.0571	0.0571	0.0529	0.0529
	C–C beam		C–C beam	
10	0.5944	0.5901	0.5475	0.5477
20	0.3166	0.3159	0.2888	0.2888
50	0.1291	0.1291	0.1174	0.1174
	C–H beam		C–H beam	
10	0.4242	0.4222	0.3898	0.3898
20	0.2203	0.2201	0.2013	0.2013
50	0.0891	0.0891	0.0813	0.0813
	C–F beam		C–F beam	
10	0.1008	0.1007	0.0917	0.0917
20	0.0508	0.0508	0.0462	0.0462
50	0.0204	0.0204	0.0185	0.0185

Table 2
First six natural frequencies of C-F porous beam for different porosity distribution, porosity coefficient and *L/h* compared with [16].

	L/h	*e*0	ω_1	ω_2	ω_3	ω_4	ω_5	ω_6
PNSD								
[16]	10	0.2	0.1003	0.5966	1.5193	1.5549	2.7936	4.2217
PRESENT			0.1003	0.5962	1.5194	1.5538	2.7921	4.2162
[16]		0.5	0.1008	0.5963	1.4379	1.5439	2.7555	4.1400
PRESENT			0.5932	0.5932	1.4379	1.5289	2.7176	4.0656
[16]		0.8	0.1050	0.6149	1.3668	1.5746	2.7800	4.1005
PRESENT			0.1046	0.6024	1.3669	1.5162	2.6352	3.8714
[16]	20	0.2	0.0505	0.3121	0.8555	1.5193	1.6282	2.6066
PRESENT			0.0505	0.3120	0.8551	1.5194	1.6269	2.5960
[16]		0.5	0.0508	0.3134	0.8572	1.4379	1.6266	2.5950
PRESENT			0.0508	0.3130	0.8543	1.4379	1.6170	2.5658
[16]		0.8	0.0530	0.3260	0.8879	1.3668	1.6761	2.6583
PRESENT			0.0529	0.3241	0.8762	1.3669	1.6390	2.5684
[16]	50	0.2	0.0202	0.1265	0.3530	0.6882	1.1360	1.5193
PRESENT			0.0202	0.1265	0.3530	0.6882	1.1301	1.5194
[16]		0.5	0.0204	0.1273	0.3550	0.6916	1.1406	1.4379
PRESENT			0.0204	0.1273	0.3548	0.6909	1.1330	1.4379
[16]		0.8	0.0212	0.1327	0.3699	0.7200	1.1857	1.3668
PRESENT			0.0212	0.1326	0.3691	0.7170	1.1720	1.3669
PNND								
[16]	10	0.2	0.0977	0.5825	1.5187	1.5229	2.7424	4.1544
PRESENT			0.0977	0.5829	1.5189	1.5252	2.7508	4.1681
[16]		0.5	0.0917	0.5471	1.4283	1.4403	2.5791	3.9080
PRESENT			0.0917	0.5472	1.4289	1.4405	2.5824	3.9119
[16]		0.8	0.0808	0.4841	1.2730	1.3680	2.3122	3.5232
PRESENT			0.0808	0.4838	1.2717	1.3680	2.3095	3.5151
[16]	20	0.2	0.0492	0.3041	0.8344	1.5193	1.5900	2.5491
PRESENT			0.0492	0.3042	0.8347	1.5193	1.5909	2.5435
[16]		0.5	0.0462	0.2856	0.6916	1.3202	1.4938	2.3953
PRESENT			0.0462	0.2856	0.7836	1.4377	1.4937	2.3878
[16]		0.8	0.0406	0.2516	0.6919	1.3213	1.3681	2.1277
PRESENT			0.0406	0.2516	0.6916	1.3202	1.3681	2.1183
[16]	50	0.2	0.0197	0.1232	0.3439	0.6705	1.1072	1.5193
PRESENT			0.0197	0.1232	0.3439	0.6707	1.1018	1.5194
[16]		0.5	0.0185	0.1157	0.3229	0.6296	1.0396	1.4379
PRESENT			0.0185	0.1157	0.3229	0.6297	1.0344	1.4379
[16]		0.8	0.0163	0.1018	0.2842	0.5544	0.9163	1.3656
PRESENT			0.0163	0.1018	0.2842	0.5545	0.9115	1.3518

Tables 3 and 4 show first six natural frequencies of porous beam with *e*0=0.5 for different boundary conditions, Skempton coefficient and *L/h*. These tables are obtained for PNSD and PNND, respectively. Results denotes that in a drained condition (*B*=0), beam has smallest fundamental frequency and by increasing Skempton coefficient, fundamental frequency increases. This is due to the fact that by increasing the Skempton coefficient, the compressibility of fluid within the pores decrease and the natural frequencies increases. In other words, if the compressibility of the pore fluid is high ($\beta \to 0$), the behavior of plate resembles that of a porous plate without fluid (drained). In this condition, the stiffness of structure has its minimum value and the least value of natural frequency is obtained. When the compressibility of pore fluid is small ($\beta \to 1$), the behavior of plate resembles that of a rigid solid, and the natural frequency has its maximum magnitude.

Table 3
First six natural frequencies of porous beam for different boundary conditions, Skempton coefficient and L/h, $e0$=0.5 (PNSD).

		PNSD					
C-F	L/h		ω_1	ω_2	ω_3	ω_4	ω_5	ω_6
	5	β=0	0.1951	1.0042	1.4379	2.3255	3.7819	4.3141
		β=0.3	0.1992	1.0190	1.4980	2.3509	3.8117	4.4943
		β=0.5	0.2023	1.0298	1.5458	2.3692	3.8331	4.6377
		β=0.7	0.2058	1.0416	1.6022	2.3889	3.8557	4.8069
	7	β=0	0.1422	0.7940	1.4379	1.9439	3.3022	4.3141
		β=0.3	0.1454	0.8080	1.4980	1.9709	3.3379	4.4943
		β=0.5	0.1477	0.8183	1.5458	1.9907	3.3637	4.6377
		β=0.7	0.1503	0.8297	1.6022	2.0122	3.3914	4.8069
	10	β=0	0.1007	0.5932	1.4379	1.5289	2.7176	4.0656
		β=0.3	0.1030	0.6050	1.4980	1.5550	2.7563	4.1139
		β=0.5	0.1047	0.6138	1.5458	1.5743	2.7847	4.1489
		β=0.7	0.1066	0.6236	1.5955	1.6022	2.8156	4.1866
C-C								
	5	β=0	0.9668	2.1540	2.8759	3.5554	5.0508	5.7526
		β=0.3	0.9781	2.1708	2.9960	3.5772	5.0753	5.9928
		β=0.5	0.9863	2.1828	3.0917	3.5926	5.0926	6.1841
		β=0.7	0.9952	2.1956	3.2044	3.6089	5.1108	6.4097
	7	β=0	0.7783	1.8406	2.8759	3.1342	4.5502	5.7526
		β=0.3	0.7903	1.8613	2.9960	3.1617	4.5821	5.9928
		β=0.5	0.7992	1.8764	3.0917	3.1814	4.6047	6.1018
		β=0.7	0.8088	1.8926	3.2025	3.2044	4.6287	6.1273
	10	β=0	0.5901	1.4770	2.6182	2.8759	3.9150	5.3130
		β=0.3	0.6010	1.4994	2.6508	2.9960	3.9553	5.3587
		β=0.5	0.6092	1.5158	2.6745	3.0917	3.9843	5.3914
		β=0.7	0.6181	1.5337	2.7001	3.2044	4.0155	5.4263
S-S								
	5	β=0	0.5238	1.4379	1.7391	3.2104	4.3141	4.7614
		β=0.3	0.5339	1.4980	1.7624	3.2385	4.4943	4.7887
		β=0.5	0.5415	1.5458	1.7793	3.2585	4.6377	4.8077
		β=0.7	0.5498	1.6022	1.7976	3.2797	4.8069	4.8274
	7	β=0	0.3896	1.3892	1.4379	2.7160	4.1905	4.3141
		β=0.3	0.3978	1.4124	1.4980	2.7503	4.2295	4.4943
		β=0.5	0.4039	1.4295	1.5458	2.7751	4.2574	4.6377
		β=0.7	0.4107	1.4482	1.6022	2.8018	4.2869	4.8069
	10	β=0	0.2792	1.0476	1.4379	2.1587	3.4784	4.3141
		β=0.3	0.2853	1.0679	1.4980	2.1938	3.5249	4.4943
		β=0.5	0.2899	1.0830	1.5458	2.2197	3.5587	4.6377
		β=0.7	0.2950	1.0996	1.6022	2.2480	3.5953	4.8069
C-S								
	5	β=0	0.7383	1.4379	1.9565	3.3864	4.3141	4.9089
		β=0.3	0.7495	1.4980	1.9766	3.4110	4.4943	4.9346
		β=0.5	0.7577	1.5458	1.9911	3.4285	4.6377	4.9526
		β=0.7	0.7667	1.6022	2.0067	3.4469	4.8069	4.9714
	7	β=0	0.5729	1.4379	1.6204	2.9305	4.3141	4.3742
		β=0.3	0.5833	1.4980	1.6428	2.9613	4.4095	4.4943
		β=0.5	0.5910	1.5458	1.6592	2.9835	4.4346	4.6377
		β=0.7	0.5995	1.6022	1.6770	3.0074	4.4612	4.8069
	10	β=0	0.4222	1.2619	1.4379	2.3918	3.7009	4.3141
		β=0.3	0.4308	1.2836	1.4980	2.4259	3.7444	4.4943
		β=0.5	0.4372	1.2997	1.5458	2.4509	3.7758	4.6377
		β=0.7	0.4443	1.3173	1.6022	2.4780	3.8097	4.8069

Table 4
First six natural frequencies of porous beam for different boundary conditions, Skempton coefficient and *L/h*, *e*0=0.5 (PNND).

		PNND						
C-F	*L/h*		ω_1	ω_2	ω_3	ω_4	ω_5	ω_6
	5	β=0	0.1789	0.9525	1.4383	2.2542	3.7284	4.309
		β=0.3	0.1863	0.9835	1.4981	2.3132	3.8076	4.492
		β=0.5	0.1922	1.0072	1.5458	2.3576	3.8664	4.6371
		β=0.7	0.199	1.0339	1.6022	2.4073	3.9313	4.8068
	7	β=0	0.1299	0.7412	1.438	1.8515	3.1992	4.3096
		β=0.3	0.1354	0.7685	1.498	1.9091	3.2832	4.4921
		β=0.5	0.1398	0.7896	1.5458	1.9531	3.3463	4.6371
		β=0.7	0.1449	0.8138	1.6022	2.0029	3.4169	4.8068
	10	β=0	0.0917	0.5472	1.4289	1.4405	2.5824	3.9119
		β=0.3	0.0957	0.5691	1.4823	1.4985	2.6644	4.0226
		β=0.5	0.0988	0.5862	1.5225	1.5459	2.7271	4.106
		β=0.7	0.1025	0.6059	1.5681	1.6022	2.7981	4.1991
C-C								
	5	β=0	0.9298	2.1209	2.8744	3.5396	5.0682	5.7375
		β=0.3	0.9554	2.1648	2.9953	3.6009	5.1439	5.9864
		β=0.5	0.9748	2.1975	3.0915	3.6464	5.2	6.1825
		β=0.7	0.9967	2.2338	3.2044	3.6969	5.262	6.4094
	7	β=0	0.7338	1.7756	2.875	3.0686	4.5019	5.7427
		β=0.3	0.7583	1.8232	2.9956	3.1374	4.5887	5.9877
		β=0.5	0.7772	1.8593	3.0915	3.189	4.6532	6.1804
		β=0.7	0.7987	1.8997	3.2044	3.2464	4.7247	6.2853
	10	β=0	0.5477	1.3952	2.5101	2.8754	3.7988	5.204
		β=0.3	0.5685	1.4413	2.5822	2.9958	3.8945	5.3208
		β=0.5	0.5847	1.4767	2.6371	3.0916	3.9666	5.4079
		β=0.7	0.6033	1.5169	2.6988	3.2044	4.0472	5.5045
S-S								
	5	β=0	0.4838	1.4207	1.6693	3.1348	4.2871	4.7364
		β=0.3	0.5031	1.4861	1.7166	3.2089	4.4747	4.8209
		β=0.5	0.5181	1.5377	1.7528	3.2639	4.6233	4.8826
		β=0.7	0.5353	1.5979	1.7939	3.3244	4.7967	4.9501
	7	β=0	0.3573	1.2895	1.4444	2.6011	4.0671	4.3125
		β=0.3	0.3722	1.3408	1.5014	2.6775	4.1743	4.4898
		β=0.5	0.3838	1.3796	1.5476	2.7355	4.2516	4.6333
		β=0.7	0.3973	1.4229	1.6027	2.8005	4.3356	4.8034
	10	β=0	0.2549	0.967	1.4331	2.0308	3.3155	4.2983
		β=0.3	0.2658	1.0058	1.4947	2.1007	3.4178	4.483
		β=0.5	0.2744	1.0359	1.5436	2.1546	3.4955	4.6298
		β=0.7	0.2844	1.0705	1.601	2.2161	3.5828	4.8023
C-S								
	5	β=0	0.6974	1.4377	1.8984	3.3427	4.3082	4.9025
		β=0.3	0.7205	1.4979	1.9463	3.4098	4.4917	4.9829
		β=0.5	0.7382	1.5457	1.9823	3.4596	4.6371	5.0421
		β=0.7	0.7583	1.6022	2.0226	3.5146	4.8068	5.1072
	7	β=0	0.5329	1.4377	1.5419	2.8395	4.2911	4.3162
		β=0.3	0.5529	1.4979	1.5897	2.9125	4.3887	4.4934
		β=0.5	0.5684	1.5458	1.6262	2.9675	4.4582	4.6374
		β=0.7	0.5862	1.6022	1.6675	3.0289	4.5348	4.8069
	10	β=0	0.3886	1.1795	1.4379	2.2708	3.5614	4.3126
		β=0.3	0.4043	1.2221	1.4979	2.3428	3.6605	4.4936
		β=0.5	0.4166	1.2551	1.5458	2.398	3.7354	4.6375
		β=0.7	0.4309	1.2929	1.6022	2.4604	3.8194	4.8069

Tables 5 and 6 show fundamental natural frequencies of porous C-F beam with *e*0=0.5 and β=0.3 for different slenderness ratio (*L/h*) and coefficient of elastic foundation. These tables are obtained for PNSD and PNND, respectively. Results denotes that by increasing the coefficient of elastic foundation, fundamental frequency increases and this is due to the fact that by increasing the elastic coefficient, stiffness of structure increases.

Table 5
Fundamental frequencies of porous C-F beam for different elastic coefficient and *L/h*, *e*0=0.5, *β*=0.3 (PNSD).

L/h	5	7	10
$k_w = 0$	0.1992	0.1454	0.1030
$k_w = 1e9$	0.4174	0.5354	0.2549
$k_w = 5e9$	0.8439	1.1161	0.5316
$k_w = 5e10$	1.4979	1.4979	1.4979

Table 6
Fundamental natural frequencies of porous C-F beam for different elastic coefficient and *L/h*, *e*0=0.5, *β*=0.3 (PNND).

L/h	5	7	10
$k_w = 0$	0.1863	0.1354	0.0957
$k_w = 1e9$	0.41158	0.5329	0.2521
$k_w = 5e9$	0.8413	1.1602	0.5303
$k_w = 5e10$	1.4977	1.4978	1.4977

As it can be seen from Fig. 2, by increasing the slenderness ratio, bending stiffness of structure and subsequently fundamental frequency decreases. Results denote that the difference between the fundamental frequencies of two porosity distributions for C-F beam is negligible compared to the other boundary conditions. Also, results denote that the natural frequency for PNSD is greater than PNND, because for PNSD, the ratio of stiffness to the mass matrix is greater than that of PNND.

Fig. 3 presents the effect of Skempton coefficient on the dimensionless fundamental frequency for *L/h* =5, $e_0 = 0.5$ and different boundary conditions. Fig. 3 shows that the fundamental frequency for C-C beam is the largest whereas in C-F beam is the smallest and by increasing the Skempton coefficient, the dimensionless fundamental frequencies for both of distributions are getting closer. This happens because, for larger values of *β*, the compressibility of pore fluid is small ($\beta \to 1$), and the behavior of plate resembles that of a rigid solid. Therefore, for larger values of *B*, the natural frequency will be identical.

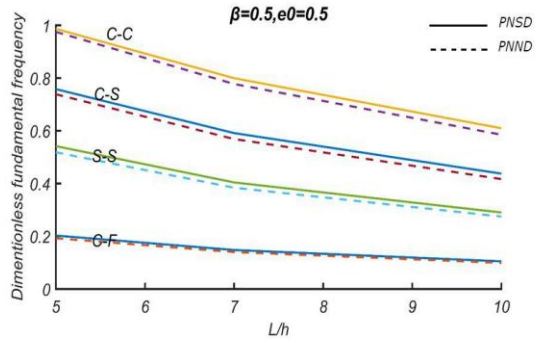

Fig.2
Dimensionless fundamental frequency of porous beam for different boundary conditions and *L/h*.

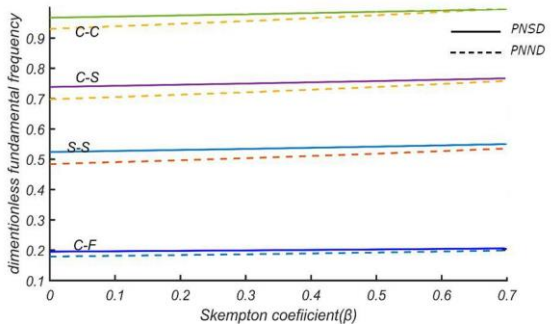

Fig.3
Dimensionless fundamental frequency of porous beam for different boundary conditions and Skempton coefficient, *L/h* =5, e_0 =0.5.

3.2 Transient vibration under an impulsive load

The transient vibration analysis of a saturated FG porous beam (L=0.5 m, b=0.1 m) is conducted and the effects of different parameters such as Skempton coefficient, porosity coefficient, slenderness ratio and boundary conditions are investigated. It is assumed that the beam is subjected to an impulsive pressure (first region), as it is depicted in (42). According to (42), the maximum magnitude of impulsive pressure at t=0.005 s is equal to 0.2 MPa [32]. The beam is excited by unloading in t=0.005 s. It is obvious that after the unloading (second region), a transient vibration which is affected by the wave propagation, reflection and interference would be occurred.

$$P_z = \begin{cases} 40t\left(\dfrac{MPa}{s}\right) & t \le 0.005 \\ 0 & t \ge 0.005 \end{cases} \tag{42}$$

The numerical results are obtained for middle point of the beam and for distribution a (PNND), unless it is noted in the specific results. Non-dimensional deflection and stresses are are $\overline{W} = \dfrac{W}{h}$, $\overline{\sigma} = \dfrac{\sigma bh}{P_z\,(t = 0.005s)L}$, respectively.

Figs. 4 and 5 show time history of midpoint transverse displacement of the simply supported beam (S-S). In these figures, the effects of Skempton coefficient and porosity coefficient are investigated, respectively. As it can be seen from Fig. 4, by increasing the Skempton coefficient, the compressibility of pore fluid decreased, and the stiffness of beam increases, hence the amplitude of vibration decreases and frequency of vibration increases, whereas by increasing the porosity coefficient for PNND, the amplitude of vibration increases and frequency of vibration decreases. This is due to the fact that by increasing the porosity coefficient, both of stiffness and mass matrices decrease, but the rate of reduction in stiffness matrix is larger than that of mass matrix for PNND.

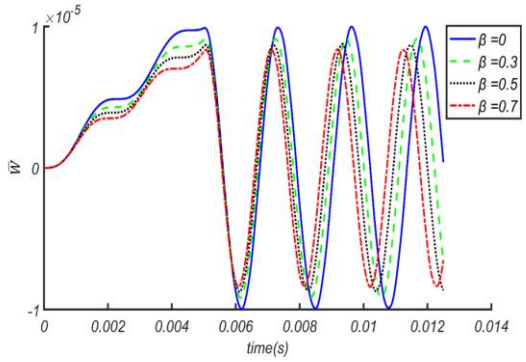

Fig.4
The effect of Skempton coefficient on time history of midpoint transverse displacement of the simply supported beam (P_z=0.2e6, e0=0.5, Distribution (a), L/h=10).

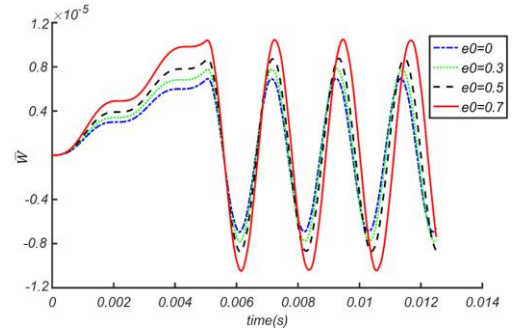

Fig.5
The effect of porosity coefficient on time history of midpoint transverse displacement of the simply supported beam (P_z =0.2e6, β =0.5, Distribution (a), L/h=10).

In Fig. 6, the effects of different boundary conditions are surveyed. As it can be seen, the highest and smallest amplitude of vibration corresponds to the C-F and C-C beam with the minimum and maximum bending stiffness, respectively.

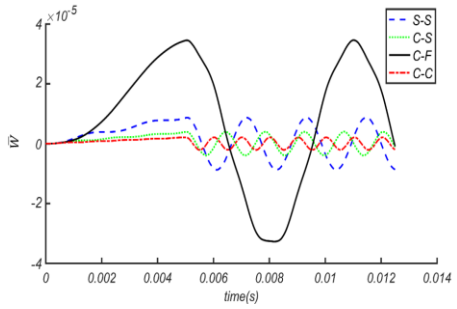

Fig.6
The effect of different boundary condition on time history of midpoint transverse displacement of the beam ($\underline{P_z}$ =0.2*e*6, Distribution (*a*), *e*0=0.5, β =0.5, *L*/*h*=10).

Figs. 7 and 8 show the effect of elastic coefficient of foundation on time history of midpoint transverse displacement and normal stress of the simply supported beam. In these results, damping coefficient of the foundation is considered to be zero $(c_d = 0)$. Results illustrate that by increasing the elastic coefficient of the foundation, the stiffness of beam increases and consequently, amplitude of transverse displacement and normal stress decrease significantly.

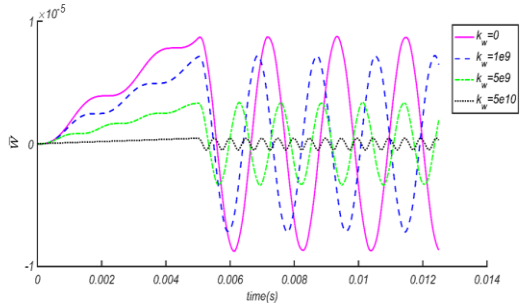

Fig.7
The effect of elastic coefficient of foundation on time history of midpoint transverse displacement of the simply supported beam (P_z =0.2*e*6, Distribution (*a*), *e*0=0.5, β =0.5, *L*/*h*=10, c_d=0).

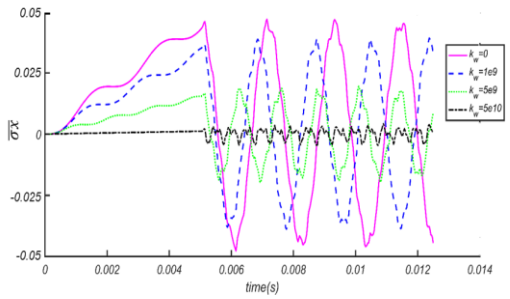

Fig.8
The effect of elastic coefficient of foundation on time history of normal stress of the simply supported beam *(*P_z =0.2*e*6, Distribution (*a*), *e*0=0.5, β=0.5, *L*/*h*=10, c_d=0, *x*=*L*/2, *z*=*h*/2).

Figs. 9 and 10 show the effect of damping coefficient of foundation on time history of midpoint transverse displacement and normal stress of the simply supported beam. In these results, elastic coefficient of the foundation is considered to be zero $(k_w = 0)$. As it can be seen from these figures, by increasing damping of the foundation, amplitude of vibration decreases and vibration of beam can be seen in three situations such as under-damped, critically-damped and over-damped.

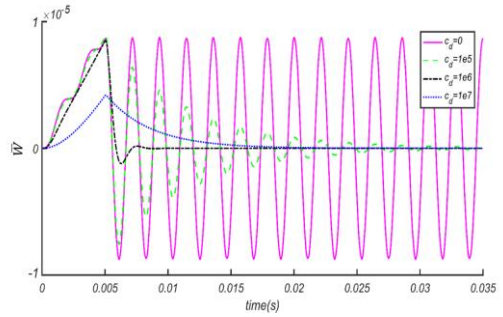

Fig.9
The effect of damping coefficient of foundation on time history of midpoint transverse displacement of the simply supported beam (P_z =0.2*e*6, Distribution (*a*), *e*0=0.5, β=0.5, *L*/*h*=10, S-S, k_w=0).

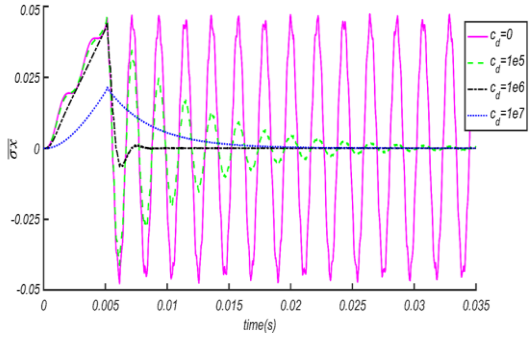

Fig.10
The effect of damping coefficient of foundation on time history of normal stress of the simply supported beam (P_z =0.2*e*6, Distribution (*a*), *e*0=0.5, *β*=0.5, *L*/*h*=10, k_w=0 *x*=*L*/2, *z*=*h*/2).

The effects of porosity and Skempton coefficients on through the thickness shear stress of a C-C beam (*x*=*L*/4) at *t*=0.005 are shown in Figs. 11 and 12. Results show that by increasing the Skempton and porosity coefficients, shear stress decreases. Also, Fig. 11 denotes that by increasing the Skempton coefficient, peak of shear stress move forward to the upper surface.

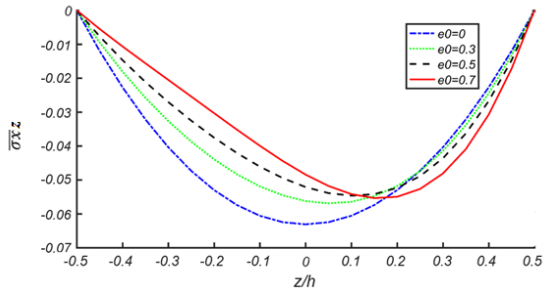

Fig.11
The effects of porosity coefficient on through the thickness shear stress of a C-C beam (P_z =0.2*e*6, Distribution (*a*), *β*=0.5, *L*/*h*=10 *x*=*L*/4).

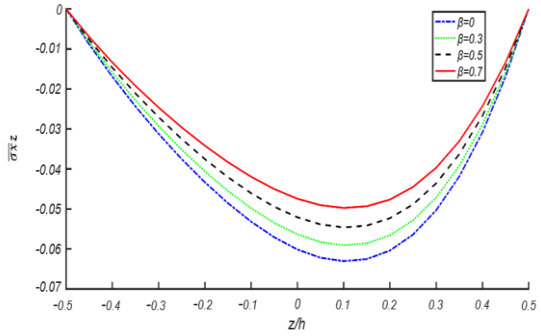

Fig.12
The effects of Skempton coefficient on the through the thickness shear stress of a C-C beam (P_z =0.2*e*6, Distribution (*a*), *e*0=0.5, *L*/*h*=10 *x*=*L*/4).

The effects of porosity coefficient on through the thickness normal stress of a C-C beam (*x*=*L*/2) at *t*=0.005 is shown in Fig. 13. Result shows that by increasing the porosity coefficient, normal stress at the upper surface increases and at the lower surface of beam decreases.

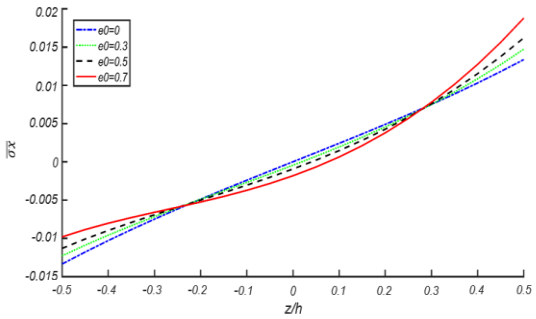

Fig.13
The effects of porosity coefficient on through the thickness normal stress of a C-C beam (P_z =0.2*e*6, Distribution (*a*), *β*=0.5, *L*/*h*=10 *x*=*L*/2).

4 CONCLUSIONS

Free and transient vibration analyses of saturated FG porous beam resting on viscoelastic foundation based on third order beam theory have been investigated for the first time. Biot constitutive law instead of Hook's law is used to model the porous behavior of beam. Lagrange equations are used to express the motion equations and the finite element and Newmark methods are used to solve the governing equations in time and space domains. The present work compared with previous studies and it shows excellent agreement. The effects of different boundary conditions, porosity and Skempton coefficients, two different porosity distribution and slenderness ratio as well as stiffness and damping coefficients of viscoelastic foundation on natural frequency and transient responses of beam have been studied. Some of main results of present study are:

In a drained condition, beam has smallest fundamental frequency and by increasing the Skempton coefficient, the fundamental frequency of the beam increases and it doesn't depend on the type of porosity distributions while by increasing the porosity coefficient, fundamental frequency in distribution 1 decreases, and in distribution 2 increases.

Fundamental frequency for C-C beam is the largest whereas in C-F beam is the smallest and by increasing the Skempton coefficient, the fundamental frequencies for both of distributions are getting closer. Also, the natural frequency for PNSD is greater than PNND.

By increasing the elastic coefficient of the foundation, amplitude of transverse displacement and normal stress decrease significantly.

By increasing damping of the foundation, amplitude of vibration decreases and vibration of beam can be seen in three situations such as under-damped, critically-damped and over-damped.

By increasing the Skempton and porosity coefficients, shear stress decreases and peak of shear stress move forward to the upper surface.

APPENDIX

$$N_{4i-3}=1-\frac{x}{l} \qquad N_{4i-2}=1-\frac{3x^2}{l^2}+\frac{2x^3}{l^3} \qquad N_{4i-1}=x-\frac{2x^2}{l}+\frac{x^3}{l^2} \qquad N_{4i}=1-\frac{x}{l}$$

$$N_{4j-3}=\frac{x}{l} \qquad N_{4j-2}=\frac{3x^2}{l^2}-\frac{2x^3}{l^3} \qquad N_{4j-1}=-\frac{x^2}{l}+\frac{x^3}{l^2} \qquad N_{4j}=\frac{x}{l}$$

$$[N]=\begin{bmatrix} N_{4i-3} & 0 & 0 & 0 & N_{4j-3} & 0 & 0 & 0 \\ 0 & N_{4i-2} & N_{4i-1} & 0 & 0 & N_{4j-2} & N_{4j-1} & 0 \\ 0 & \frac{\partial N_{4i-2}}{\partial x} & \frac{\partial N_{4i-1}}{\partial x} & 0 & 0 & \frac{\partial N_{4j-2}}{\partial x} & \frac{\partial N_{4j-1}}{\partial x} & 0 \\ 0 & 0 & 0 & N_{4i} & 0 & 0 & 0 & N_{4j} \end{bmatrix}$$

$$[B]=\begin{bmatrix} \frac{\partial N_{4i-3}}{\partial x} & 0 & 0 & 0 & \frac{\partial N_{4j-3}}{\partial x} & 0 & 0 & 0 \\ 0 & 0 & 0 & \frac{\partial N_{4i}}{\partial x} & 0 & 0 & 0 & \frac{\partial N_{4j}}{\partial x} \\ 0 & \frac{\partial^2 N_{4i-2}}{\partial x^2} & \frac{\partial^2 N_{4i-1}}{\partial x^2} & 0 & 0 & \frac{\partial^2 N_{4j-2}}{\partial x^2} & \frac{\partial^2 N_{4j-1}}{\partial x^2} & 0 \\ 0 & \frac{\partial N_{4i-2}}{\partial x} & \frac{\partial N_{4i-1}}{\partial x} & N_{4i} & 0 & \frac{\partial N_{4j-2}}{\partial x^2} & \frac{\partial N_{4j-1}}{\partial x} & N_{4j} \end{bmatrix}$$

$$\left[\bar{N}\right]=\begin{bmatrix} 0 & 0 & 0 & 0 & 0 & 0 & 0 & 0 \\ 0 & N_{4i-2} & N_{4i-1} & 0 & 0 & N_{4j-2} & N_{4j-1} & 0 \\ 0 & 0 & 0 & 0 & 0 & 0 & 0 & 0 \\ 0 & 0 & 0 & 0 & 0 & 0 & 0 & 0 \end{bmatrix}$$

REFERENCES

[1] Hromadová L., 2009, *Thermal Pressurization of Pore Fluid During Earthquake Slip*, Comenius University, Bratislava.

[2] Biot M.A., 1955, Theory of elasticity and consolidation for a porous anisotropic solid, *Journal of Applied Physics* **26**(2): 182-185.

[3] Theodorakopoulos D.D., Beskos D.E., 1994, Flexural vibrations of poroelastic plates, *Acta Mechanica* **103**(1-4): 191-203.

[4] Leclaire P., Horoshenkov K.V., Swift M.J., Hothersall D.C., 2001, The vibrational response of a clamped rectangular porous plate, *Journal of Sound and Vibration* **247**(1): 19-31.

[5] Magnucki K., Stasiewicz P., 2004, Elastic buckling of a porous beam, *Journal of Theoretical and Applied Mechanics* **42**(4): 859-868.

[6] Magnucka-Blandzi E., 2008, Axi-symmetrical deflection and buckling of circular porous-cellular plate, *Thin-Walled Structures* **46**(3): 333-337.

[7] Magnucka-Blandzi E., Magnucki K., 2007, Effective design of a sandwich beam with a metal foam core, *Thin-Walled Structures* **45**(4): 432-438.

[8] Debowski D., Magnucki K., 2006, Dynamic stability of a porous rectangular plate, *PAMM* **6**(1): 215-216.

[9] Mojahedin A., Joubaneh E.F., Jabbari M., 2014, Thermal and mechanical stability of a circular porous plate with piezoelectric actuators, *Acta Mechanica* **225**(12): 3437-3452.

[10] Jabbari M., Mojahedin A., Khorshidvand A.R., Eslami M.R., 2013, Buckling analysis of a functionally graded thin circular plate made of saturated porous materials, *Journal of Engineering Mechanics* **140**(2): 287-295.

[11] Jabbari M., Mojahedin A., Haghi M., 2014, Buckling analysis of thin circular FG plates made of saturated porous-soft ferromagnetic materials in transverse magnetic field, *Thin-Walled Structures* **85**: 50-56.

[12] Ebrahimi F., Mokhtari M., 2015, Transverse vibration analysis of rotating porous beam with functionally graded microstructure using the differential transform method, *Journal of the Brazilian Society of Mechanical Sciences and Engineering* **37**(4):1435-1444.

[13] Ebrahimi F., Jafari A., 2018, A four-variable refined shear-deformation beam theory for thermo-mechanical vibration analysis of temperature-dependent FGM beams with porosities, *Mechanics of Advanced Materials and Structures* **25**(3): 212-224.

[14] Ebrahimi F., Ghasemi F., Salari E., 2016, Investigating thermal effects on vibration behavior of temperature-dependent compositionally graded Euler beams with porosities, *Meccanica* **51**(1): 223-249.

[15] Chen D., Yang J., Kitipornchai S., 2015, Elastic buckling and static bending of shear deformable functionally graded porous beam, *Composite Structures* **133**: 54-61.

[16] Chen D., Yang J., Kitipornchai S., 2016, Free and forced vibrations of shear deformable functionally graded porous beams, *International Journal of Mechanical Sciences* **108**: 14-22.

[17] Chen D., Kitipornchai S., Yang J., 2016, Nonlinear free vibration of shear deformable sandwich beam with a functionally graded porous core, *Thin-Walled Structures* **107**: 39-48.

[18] Arshid E., Khorshidvand A.R., 2018, Free vibration analysis of saturated porous FG circular plates integrated with piezoelectric actuators via differential quadrature method, *Thin-Walled Structures* **125**(1): 220-233.

[19] Galeban M.R., Mojahedin A., Taghavi Y., Jabbari M., 2016, Free vibration of functionally graded thin beams made of saturated porous materials, *Steel and Composite Structures* **21**(5): 999-1016.

[20] Grygorowicz M., Magnucki K., Malinowski M., 2015, Elastic buckling of a sandwich beam with variable mechanical properties of the core, *Thin-Walled Structures* **87**: 127-132.

[21] Ghorbanpour Arani A., Khani M., Khoddami Maraghi Z., 2018, Dynamic analysis of a rectangular porous plate resting on an elastic foundation using high-order shear deformation theory, *Journal of Vibration and Control* **241**(6): 3698-3713.

[22] Ghorbanpour Arani A., Khoddami Maraghi Z., Khani M., Alinaghian I., 2017, Free vibration of embedded porous plate using third-order shear deformation and poroelasticity theories, *Journal of Engineering* **2017**: 1474916.

[23] Ghorbanpour Arani A., Zamani M.H., 2018, Nonlocal free vibration analysis of FG-porous shear and normal deformable sandwich nanoplate with piezoelectric face sheets resting on silica aerogel foundation, *Arabian Journal for Science and Engineering* **43**(9): 4675-4688.

[24] Magnucka-Blandzi E., 2009, Dynamic stability of a metal foam circular plate, *Journal of Theoretical and Applied Mechanics* **47**: 421-433.

[25] Mojahedin A., Jabbari M., Khorshidvand A.R., Eslami M.R., 2016, Buckling analysis of functionally graded circular plates made of saturated porous materials based on higher order shear deformation theory, *Thin-Walled Structures* **99**: 83-90.
[26] Ebrahimi F., Habibi S., 2016, Deflection and vibration analysis of higher-order shear deformable compositionally graded porous plate, *Steel and Composite Structures* **20**(1): 205-225.
[27] Zimmerman R.W., 2000, Couplingin poroelasticity and thermoelasticity, *International Journal of Rock Mechanics and Mining Sciences* **37**: 79-87.
[28] Detournay E., Cheng A.H.D., 1993, Fundamentals of poroelasticity, *Analysis and Design Methods* **1993**:113-171.
[29] Peng X.Q., Lam K.Y., Liu G.R., 1998, Active vibration control of composite beams with piezoelectrics: a finite element model with third order theory, *Journal of Sound and Vibration* **209**(4): 635-650.
[30] Meyers M., Chawla K., 1999, *Mechanical Behavior of Materials*, Prentice Hall, Inc, Section.
[31] Majzoobi GH., 2013, *Concepted and Applications of Finite Element Method*, Bu Ali Sina University of Technology Publication Center.
[32] Shakeri M., Akhlaghi M., Hoseini S. M., 2006, Vibration and radial wave propagation velocity in functionally graded thick hollow cylinder, *Composite Structures* **76**(1-2): 174-181.